universe

MDPI

Article

An Idealized Uniform Charge-Partition Baseline for Nuclear Fragment Multiplicity Distributions in High-Energy Nuclear Fragmentation

Jia-Yu Chen [1,2,*] and Chun-Hua Shi [1,2,*]

[1] Basic Physics Section and Comprehensive Physics Laboratory, Department of Biomedical Engineering, Changzhi Medical College, Jiefang East Street, Changzhi 046000, China
[2] Key Laboratory of Medical Electronics and Rehabilitation Device Engineering of Changzhi City, Changzhi Medical College, Jiefang East Street, Changzhi 046000, China
* Correspondence: chenjiayu@czmc.edu.cn (J.-Y.C.); shi-chunhua@czmc.edu.cn (C.-H.S.)

Abstract

Collective expansion is a hallmark of high-energy nuclear collisions, yet its interplay with the subsequent fragmentation process remains highly complex. Because isolating dynamical signals from raw data is challenging, this paper proposes a combinatorial baseline framework for nuclear fragmentation based on the theory of integer partitions, in which the charge-number fragmentation channels of a nucleus are mathematically equivalent to partitions of a positive integer. When only charge-number conservation is considered, a beam nucleus with charge number Z_{beam} has $p(Z_{\mathrm{beam}})$ possible fragmentation modes. To establish an idealized zero-order reference, we introduce the assumption that all fragmentation channels are equiprobable. Based on this framework, we compute the exact combinatorial fragmentation baseline for the future Electron-Ion Collider (EIC). We calculate the multiplicity distributions of nuclear fragments over all fragmentation channels of the gold ($^{197}_{79}$Au) nucleus, as well as those of nuclear fragments with charges of $Z = 1$ to $Z = 12$. Then, for $Z_{\mathrm{beam}} = 6$ to 100, the fragmentation channels obtained from the partition method and the multiplicity distributions of nuclear fragments with $Z = 1$ and 2 are studied to extract the empirical Tsallis fitting parameters (q and T_q). The dependences of q and T_q on Z_{beam} are analyzed, yielding $q = 1 - aZ_{\mathrm{beam}}^{-b}$ and $T_q = A\sqrt{Z_{\mathrm{beam}}} + B$ for $Z_{\mathrm{beam}} \geq 20$, where a, b, A, and B are fit parameters. The result of $q < 1$ mathematically reflects a compact-support distribution intrinsic to the finite combinatorial space, rather than directly establishing the genuine nonextensive thermodynamic properties of the physical system. Because real fragmentation yields are strongly influenced by collective dynamics, isotope composition, and phase-space weights, the deviations of experimental data from this idealized combinatorial baseline can serve as a crucial reference. These deviations encapsulate the combined non-combinatorial physical effects, providing a rigorous starting point for isolating and investigating genuine collective dynamics in future studies.

Keywords: nuclear fragmentation; multiplicity distribution; integer partition; finite-size effect; Tsallis entropy; effective temperature; Electron–Ion Collider (EIC)

Check for updates

Academic Editor: Máté Csanád

Received: 28 September 2026
Revised: 12 November 2026
Accepted: 14 November 2026
Published: 17 November 2026

Copyright: © 2026 by the authors. Licensee MDPI, Basel, Switzerland. This article is an open access article distributed under the terms and conditions of the Creative Commons Attribution (CC BY) license.

1. Introduction

The high-energy Electron-Ion Collider (EIC) is a next-generation flagship large-scale scientific facility [1–3]. It is currently being planned by the international nuclear physics community. Its central physics mission is threefold. First, it will use point-like lepton

probes in ultrahigh-luminosity deep inelastic scattering. This will enable unprecedented high-precision three-dimensional imaging of the partonic structure of nuclei. Second, it will systematically study strong-interaction corrections in the nuclear medium. These corrections include parton energy loss and parton recombination. Third, it will address a long-standing central scientific question. This question concerns the quark-gluon distributions in nuclei. The world's first EIC facility is currently under construction at Brookhaven National Laboratory in the United States. It is expected to begin official data taking in 2027. China has also included the next-generation polarized Electron-Ion Collider in China (EicC) in its mid- and long-term plans for major nuclear physics facilities [4–6]. This field will be one of the core frontiers of nuclear physics research over the next two decades.

In a typical electron-ion deep inelastic scattering (DIS) reaction [7–10], the incident high-energy electron transfers a large momentum, far exceeding the nucleon binding energy, to a parton inside the target nucleus. The struck parton rapidly escapes from the nucleus carrying extremely high transverse momentum. The nucleus, initially in a globally bound state, undergoes violent fragmentation driven by local energy deposition and momentum imbalance. This complex process is strongly influenced by radial collective expansion and ultimately produces numerous final-state charged fragments with various charge and mass numbers. The theoretical description of nuclear fragmentation has long been a challenging problem in nuclear physics. Various theoretical frameworks have been developed, including transport models, cascade fragmentation models, and statistical fragmentation models. However, these models generally require the introduction of at least five phenomenological parameters, such as temperature, fragmentation excitation energy, fragment formation energy, etc., to fit experimental data. Predictions for the yield of the same fragmentation channel often differ among models by factors of several or even orders of magnitude. To date, a universal, first-principles-based statistical baseline that isolates pure conservation laws from complex collective dynamics has not yet been firmly established.

Traditional statistical fragmentation theory generally assumes that the phase-space distribution of final-state fragments follows extensive Boltzmann–Gibbs statistics and that the entropy strictly obeys extensivity, i.e., the total entropy of the whole system equals the simple sum of the entropies of its independent subsystems [11–14]. In recent years, however, extensive data accumulated from numerous heavy-ion collision experiments at the Relativistic Heavy Ion Collider (RHIC) and the Large Hadron Collider (LHC) have consistently indicated that the multiplicity and transverse-momentum distributions of final-state particles deviate markedly from the simple exponential form of the Boltzmann distribution and exhibit pronounced inverse-power-law tails. Such features cannot arise naturally in traditional extensive statistics and can be described with high precision only by introducing the Tsallis distribution within nonextensive statistical mechanics [15–20]. To date, however, no consensus has been reached on the physical origin of the nonextensivity observed in high-energy collisions. Most existing studies attribute it vaguely to long-range correlations in the partonic system, strong dynamical fluctuations, or finite-size effects in strongly interacting systems. A clear, quantitatively calculable geometric–statistical correspondence has long been lacking, and the Tsallis parameters extracted from data are often treated merely as empirical fitting tools without a transparent microscopic baseline.

To address this gap, this paper proposes an idealized combinatorial baseline framework. Rather than attempting to fully describe the complex physical dynamics, we isolate the sole and most basic global constraint of charge-number conservation. Under this constraint, all physically allowed final states of the nuclear fragmentation process correspond exactly one-to-one to the set of all unordered partitions of the positive integer equal to the nuclear charge number. Each unordered partition represents a combination of final-state fragments with different charge numbers, and each corresponds to an independent, physically allowed

nuclear fragmentation channel. As a necessary prior assumption to establish a zero-order reference devoid of dynamical bias, we assume that all fragmentation channels are exactly equiprobable. The statistical properties of such equiprobable partitions mathematically exhibit a compact-support distribution that naturally differs from extensive statistics. This baseline provides a geometrical-statistical reference point, without claiming to directly explain the complete physical origin of nuclear fragmentation.

The collective expansion of the collision system, particularly the radial collective flow, is one of primary drivers of the nuclear fragmentation mechanism and significantly alters the final-state multiplicities. While the combinatorial baseline proposed here neglects these dynamical effects (along with isotope composition and phase-space weights), it provides a crucial benchmark. Should the experimentally measured fragment multiplicity distribution deviate from the idealized partitioning baseline presented in this work, such a deviation would indicate the presence of non-combinatorial physical effects. By systematically comparing experimental data with this baseline, future studies can isolate these deviations, thereby providing a valuable starting point for extracting key collective dynamical information, such as the magnitude of the radial collective flow, when combined with advanced transport or hydrodynamic models.

This paper is organized as follows. Section 2 investigates integer partitions and equiprobable nuclear fragmentation, focusing on the gold beam nucleus ($^{197}_{79}$Au) at the EIC, whose charge number is $Z_{\mathrm{beam}} = 79$. It mainly addresses the multiplicity distributions of nuclear fragments with different charge numbers (Z_F or $Z = 1$–12). Section 3 presents the dependences of the empirical Tsallis fitting parameters (q and T_q) on Z_{beam}, extracted from the multiplicity distributions of nuclear fragments with $Z = 1$ and 2. Section 4 discusses the significance and application prospects of the partition method. Section 5 provides the summary and conclusions.

2. Integer Partitions and the Equiprobable Combinatorial Baseline

The unordered partition of integers is a classic core problem in number theory [21–23], with a history spanning more than three centuries. It was first proposed by Leibniz and later developed by Euler, Hardy, Ramanujan, and others. It concerns the number of ways to express a positive integer m as a sum of positive integers, irrespective of order. The central statistic in partition theory, $p(m,k)$, is defined as the number of ways to partition m into exactly k positive integers. In the nuclear fragmentation context considered here, this corresponds to the number of independent fragmentation channels in which a nucleus with charge number Z_{beam} (analogous to m) breaks into exactly N_F final-state fragments (analogous to k), where N_F is the fragment multiplicity. This represents a formal mathematical mapping designed to construct an idealized zero-order combinatorial baseline. The definition of an unordered partition is adopted here because the order in which fragments are produced does not affect the classification of final-state fragmentation channels, and only the set of charge-number fragments present in the final state matters. Therefore, the ordering of the numbers in the partition need not be considered, avoiding double counting of mathematically equivalent charge partitions.

2.1. Formula for Partitions

The exact values of $p(m,k)$ can be obtained from the standard recurrence relation for integer partitions [21]. This recurrence, first proposed by Euler in the 18th century, is the standard and most rigorous method in number theory for computing partition numbers:

$$p(m,k) = p(m-1,k-1) + p(m-k,k). \tag{1}$$

In the nuclear fragmentation context, the combinatorial analogy of this recurrence is as follows. The total number of fragmentation channels for a nucleus with charge number $Z_{\text{beam}} = m$ to break into $N_F = k$ fragments equals the sum of the numbers of two mutually exclusive and exhaustive classes of fragmentation channels. The first class contains at least one fragment with charge number 1; removing this fragment of charge 1 leaves a fragmentation of a nucleus with charge number $m - 1$ into $k - 1$ fragments. In the second class, all fragments have charge numbers ≥ 2; subtracting 1 from the charge number of each fragment leaves a fragmentation of a nucleus with charge number $m - k$ into k fragments. These two classes are disjoint and together exhaust all possible charge combinations, so the combinatorial logic of the recurrence is fully self-consistent.

The boundary conditions of this recurrence have a clear combinatorial interpretation. For $k = 1$, $p(m, 1) = 1$, corresponding to the intact nucleus with no fragmentation occurring. For $k = m$, $p(m, m) = 1$, corresponding to complete fragmentation into m fragments of charge number 1. For $k > m$, $p(m, k) = 0$, since charge conservation forbids fragmenting a nucleus of charge number m into more than m positively charged fragments. In terms of generating functions [21], $p(m, k)$ can be expressed as the coefficient in the expansion

$$\sum_{m=k}^{\infty} p(m,k)x^m = x^k \prod_{i=1}^{k} \frac{1}{1-x^i}, \tag{2}$$

where i runs from 1 to k. Equivalently, $p(m, k)$ is the coefficient of x^{m-k} in the formal power series, i.e.,

$$\prod_{i=1}^{k} \frac{1}{1-x^i} = \sum_{m=k}^{\infty} p(m,k)x^{m-k} = 1 + p(k+1,k)x + p(k+2,k)x^2 + \cdots, \tag{3}$$

which rigorously guarantees, at the algebraic level, the completeness of the partition-number calculation and ensures that no mathematically allowed charge combination is omitted.

For large m values, number theory also provides the Hardy–Ramanujan asymptotic formula [21], which gives a rapid estimate of the order of magnitude of the total partition number ($p(m) = \sum_{k=1}^{m} p(m, k)$):

$$p(m) \sim \frac{1}{4m\sqrt{3}} \exp\left(\pi\sqrt{\frac{2m}{3}}\right). \tag{4}$$

For $m = 100$, this leading asymptotic term already yields the correct order of magnitude, with a relative error of only a few percent; including the first correction term further improves the accuracy. This formula can therefore serve as a quick consistency check on the computed total partition number for a nucleus with a large charge number.

It should be noted that when the above method is applied to nuclear partitions or fragmentation, our baseline model considers exclusively the global constraint of charge-number conservation, that is, only the Z_{beam} protons are partitioned, while the $A - Z_{\text{beam}}$ neutrons are not, where A is the mass number of the nucleus. Because real fragmentation yields are strongly influenced by complex dynamics, isotope composition, and collective expansion, omitting the neutrons and other phase-space weights allows us to isolate the pure combinatorial charge partitions. If the $A - Z_{\text{beam}}$ neutrons were also partitioned, additional constraints from the nuclide chart would have to be imposed on the resulting nuclides. Partitioning both the Z_{beam} protons and the $A - Z_{\text{beam}}$ neutrons simultaneously would greatly increase the total number of fragmentation channels, making the calculation far more complex and the experimental detection more difficult. For simplicity, this paper considers only the partitioning of the Z_{beam} protons as our idealized reference.

2.2. Number of Parts and the Corresponding Partition Number

The gold nucleus, with charge number $Z_{\text{beam}} = 79$, is among the most commonly used heavy nuclear materials in nuclear fragmentation experiments. Gold-nucleus fragmentation experiments at the EIC would provide an excellent opportunity for high-energy nuclear fragmentation research. Owing to its high atomic number and large nucleon number, the fragmentation process produces a rich variety of final-state fragments, making gold an ideal subject for studying the statistical laws of nuclear fragmentation. Based on the equivalence between integer partitions and nuclear fragmentation channels established above, all possible combinatorial charge partitioning channels of gold nuclei can be calculated exactly. In this framework, the number of parts (k) corresponds to the fragment multiplicity (N_F), and the partition number ($p(79,k)$) gives the multiplicity distribution ($\mathrm{d}n/\mathrm{d}N_F$, where n is the number of events with multiplicity N_F).

We computed $p(79,k)$ for all k (N_F) from 1 to 79 with $m = 79$, i.e., $Z_{\text{beam}} = 79$ for $^{197}_{79}$Au. The results are listed in Table 1. The total number of fragmentation channels, $\sum_{N_F=1}^{79} p(79,N_F) = 13{,}848{,}650$, is in complete agreement with the accepted values of $p(79,k)$ in OEIS A008284 [24], confirming the accuracy of the tabulated data.

The data show that $p(79,k)$ increases rapidly with increasing k, reaches a peak at $k = 15$ [$p(79,15) = 918{,}851$, accounting for 6.6349%], and then decreases rapidly at first and slowly thereafter, exhibiting a long tail in the high-k region. The overall distribution is unimodal and asymmetric, mainly concentrated in $k = 11$–20 (58.3899%). Contributions from the other segments are as follows: $k = 1$–10 accounts for 8.7166%, 21–30 for 26.2821%, and 31–40 for 5.5564%; the first 40 terms account for 98.9401%, while the tail from 41 to 79 accounts for only about 1.0599%.

With N_F on the horizontal axis and $p(79,N_F)$ (equivalently, $\mathrm{d}n/\mathrm{d}N_F$) on the vertical axis, the multiplicity distribution is plotted in Figure 1. It is clearly unimodal, peaks at $N_F = 15$, and exhibits a pronounced long tail at high N_F values. This shape is mathematically distinct from the Poisson or Gaussian forms typically used in extensive statistical physics.

To empirically characterize the shape of this exact combinatorial distribution, we fit the region to the right of the peak using a Tsallis probability density function [15–20],

$$p(N_F) = P(0)\left[1 - \frac{(1-q)N_F}{T_q}\right]^{\frac{1}{1-q}}, \tag{5}$$

where $P(0)$ is the normalization constant and q and T_q are treated as empirical fitting parameters. The Tsallis fit is shown by the solid curve in Figure 1, with the fitted parameters given therein. The fit yields $q = 0.7958 \pm 0.0212$ and $T_q = 13.1830 \pm 0.6228$. For $q < 1$, the Tsallis distribution does not exhibit a power-law tail; instead, it abruptly terminates at a finite endpoint of $N_F = T_q/(1-q)$, corresponding to a compact-support distribution. We emphasize that this $q < 1$ feature mathematically reflects the finite combinatorial space (since the exact distribution extends to $N_F = 79$, while the fitted endpoint is approximately $N_F = 64.6$). It represents the truncation of the combinatorial phase space, rather than establishing the genuine nonextensive thermodynamic properties of the physical system. Although the Tsallis probability density function does not provide a complete description of the multiplicity distributions for fragments with different charge numbers, it reproduces the trend on the high-multiplicity side of the peak. However, it fails on the left-hand side of the peak.

To fit the histogram over the full N_F range, we also use the Gumbel probability density function [25–28]:

$$p(N_F) = C_0 \exp\left[-\frac{N_F - \mu}{\beta} - \exp\left(-\frac{N_F - \mu}{\beta}\right)\right], \tag{6}$$

where C_0 is the normalization constant and μ and β are free parameters. The result obtained by fitting with the Gumbel probability density function is shown by the dashed curve in Figure 1, with the fitted parameters given therein. The Gumbel probability density function corresponds to an asymptotic distribution for maxima or minima, and the combinatorial multiplicity distribution approximately satisfies this condition.

Because the histogram values are exact and carry no uncertainties, a χ^2 goodness-of-fit test cannot be performed. Instead, we introduce a pseudo "relative error" ($\sqrt{\mathrm{d}n/\mathrm{d}N_F}$) to compare the fits of the two functions. The comparison shows that the Gumbel probability density function describes the data much better than the Tsallis probability density function. This result is also intuitive.

Tables 2–13 list the multiplicity distributions of nuclear fragments with $Z = 1$–12 produced in the combinatorial partitioning of gold nuclei, and the corresponding histograms and Tsallis fitted curves are shown in Figure 2a–i. A common feature is that zero-multiplicity events dominate, and $\mathrm{d}n/\mathrm{d}N_F$ (or $\mathrm{d}n/\mathrm{d}N_Z$) decreases rapidly with increasing multiplicity. As Z increases, the empirical fitting parameter (q) decreases slowly or remains nearly constant, always deviating significantly from 1, whereas the empirical fitting parameter (T_q) decreases rapidly. These q values also indicate that the baseline distributions exhibit compact-support features.

In general, the fitted q deviates from 1 with high significance and remains below 1 for all fit ranges considered [$q_{\min} = 0.796$ for $p(79, N_F)$, and $q = 0.948$–0.949 for all $Z = 1$–12]. It is important to distinguish this purely mathematical result from the Tsallis parameters extracted from real experimental data. In genuine physical fragmentation processes, a fitted parameter $q > 1$ often reflects non-equilibrium dynamics, long-range correlations, or collective effects. In contrast, the $q < 1$ obtained here is a strict mathematical consequence of the finite integer partition space. Consequently, the q values derived from our combinatorial baseline represent a fundamentally different physical context and are not directly comparable to the q parameters reported in the literature for real light-nucleus fragmentation.

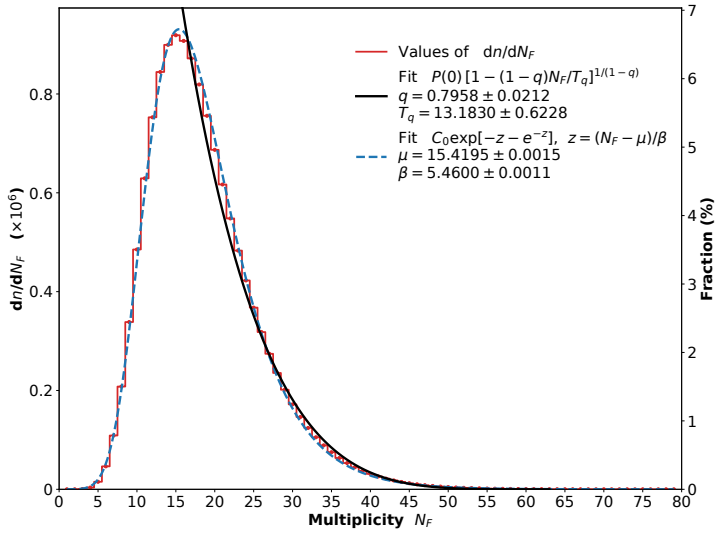


Figure 1. Multiplicity distribution of nuclear fragments, $\mathrm{d}n/\mathrm{d}N_F$, obtained from the combinatorial baseline for the fragmentation of $^{197}_{79}$Au. The histogram shows the exact values of $\mathrm{d}n/\mathrm{d}N_F$ obtained from the equiprobable charge-partition method. The right vertical axis gives the percentage fraction (%). The solid curve is the fit to the range $N_F = 15$–63 using the Tsallis function $P(N_F) = P(0)[1 - (1 - q)N_F/T_q]^{1/(1-q)}$, with the free parameters q and T_q given in the legend and $P(0) = (3.8687 \pm 0.0063) \times 10^6$. The maximum $N_F = 63$ is used in the fit because the compact-support distribution is truncated at $T_q/(1 - q) = 13.183/0.2042 = 64.559$. The dashed curve is the fit over the entire N_F range using the Gumbel function $P(N_F) = C_0 \exp(-z - e^{-z})$ with $z = (N_F - \mu)/\beta$, where

the free parameters μ and β are given in the legend and $C_0 = (2.5308 \pm 0.0008) \times 10^6$. Because the combinatorial baseline yields exact and error-free values, standard statistical p-value tests cannot be used to compare the goodness of fit. However, to estimate the parameter uncertainties, we apply the χ^2 profile method by artificially assigning Poisson statistical uncertainties ($\sqrt{\mathrm{d}n/\mathrm{d}N_F}$) to the exact baseline yields. The reported uncertainties assume a 1σ deviation corresponding to a 68.3% confidence level.

Table 1. Multiplicity distribution of nuclear fragments, $\mathrm{d}n/\mathrm{d}N_F$, produced in $^{197}_{79}$Au fragmentation.

N_F	$\mathrm{d}n/\mathrm{d}N_F$	Fraction (%)	N_F	$\mathrm{d}n/\mathrm{d}N_F$	Fraction (%)
1	1	0.0000	41	26,015	0.1879
2	39	0.0003	42	21,637	0.1562
3	520	0.0038	43	17,977	0.1298
4	3549	0.0256	44	14,883	0.1075
5	15,257	0.1102	45	12,310	0.0889
6	46,461	0.3355	46	10,143	0.0732
7	108,869	0.7861	47	8349	0.0603
8	207,945	1.5016	48	6842	0.0494
9	338,484	2.4442	49	5604	0.0405
10	485,315	3.5044	50	4565	0.0330
11	629,281	4.5440	51	3718	0.0268
12	752,802	5.4359	52	3010	0.0217
13	844,504	6.0981	53	2436	0.0176
14	899,427	6.4947	54	1958	0.0141
15	918,851	6.6349	55	1575	0.0114
16	907,376	6.5521	56	1255	0.0091
17	871,908	6.2960	57	1002	0.0072
18	819,205	5.9154	58	792	0.0057
19	755,880	5.4581	59	627	0.0045
20	686,983	4.9606	60	490	0.0035
21	616,825	4.4540	61	385	0.0028
22	548,134	3.9580	62	297	0.0021
23	483,076	3.4883	63	231	0.0017
24	422,664	3.0520	64	176	0.0013
25	367,697	2.6551	65	135	0.0010
26	318,199	2.2977	66	101	0.0007
27	274,251	1.9803	67	77	0.0006
28	235,435	1.7001	68	56	0.0004
29	201,512	1.4551	69	42	0.0003
30	171,928	1.2415	70	30	0.0002
31	146,358	1.0568	71	22	0.0002
32	124,246	0.8972	72	15	0.0001
33	105,286	0.7603	73	11	0.0001
34	88,995	0.6426	74	7	0.0001
35	75,108	0.5423	75	5	0.0000
36	63,231	0.4566	76	3	0.0000
37	53,162	0.3839	77	2	0.0000
38	44,579	0.3219	78	1	0.0000
39	37,337	0.2696	79	1	0.0000
40	31,185	0.2252			

Table 2. Multiplicity distribution, $dn/dN_{Z=1}$, of nuclear fragments with $Z = 1$ produced in $^{197}_{79}$Au fragmentation.

$N_{Z=1}$	$dn/dN_{Z=1}$	Fraction (%)	$N_{Z=1}$	$dn/dN_{Z=1}$	Fraction (%)
0	1,716,486	12.3946	40	5170	0.0373
1	1,512,301	10.9202	41	4378	0.0316
2	1,330,772	9.6094	42	3660	0.0264
3	1,170,827	8.4544	43	3094	0.0223
4	1,028,764	7.4286	44	2573	0.0186
5	903,811	6.5263	45	2167	0.0156
6	792,906	5.7255	46	1794	0.0130
7	695,578	5.0227	47	1507	0.0109
8	609,237	4.3993	48	1238	0.0089
9	533,623	3.8532	49	1039	0.0075
10	466,610	3.3694	50	847	0.0061
11	408,046	2.9465	51	708	0.0051
12	356,169	2.5719	52	574	0.0041
13	310,962	2.2454	53	478	0.0035
14	270,928	1.9563	54	383	0.0028
15	236,131	1.7051	55	320	0.0023
16	205,343	1.4828	56	253	0.0018
17	178,651	1.2900	57	210	0.0015
18	155,038	1.1195	58	165	0.0012
19	134,647	0.9723	59	137	0.0010
20	116,600	0.8420	60	105	0.0008
21	101,066	0.7298	61	88	0.0006
22	87,331	0.6306	62	66	0.0005
23	75,547	0.5455	63	55	0.0004
24	65,121	0.4702	64	41	0.0003
25	56,224	0.4060	65	34	0.0002
26	48,342	0.3491	66	24	0.0002
27	41,646	0.3007	67	21	0.0002
28	35,717	0.2579	68	14	0.0001
29	30,701	0.2217	69	12	0.0001
30	26,252	0.1896	70	8	0.0001
31	22,519	0.1626	71	7	0.0001
32	19,196	0.1386	72	4	0.0000
33	16,424	0.1186	73	4	0.0000
34	13,959	0.1008	74	2	0.0000
35	11,914	0.0860	75	2	0.0000
36	10,087	0.0728	76	1	0.0000
37	8591	0.0620	77	1	0.0000
38	7245	0.0523	78	0	0.0000
39	6153	0.0444	79	1	0.0000

Table 3. Multiplicity distribution, $dn/dN_{Z=2}$, of nuclear fragments with $Z = 2$ produced in $^{197}_{79}$Au fragmentation.

$N_{Z=2}$	$dn/dN_{Z=2}$	Fraction (%)	$N_{Z=2}$	$dn/dN_{Z=2}$	Fraction (%)
0	3,228,787	23.3148	20	9548	0.0689
1	2,501,599	18.0638	21	6754	0.0488
2	1,932,575	13.9550	22	4740	0.0342
3	1,488,484	10.7482	23	3301	0.0238
4	1,142,860	8.2525	24	2277	0.0164
5	874,656	6.3158	25	1555	0.0112
6	667,131	4.8173	26	1052	0.0076
7	507,059	3.6614	27	703	0.0051
8	383,994	2.7728	28	463	0.0033
9	289,685	2.0918	29	302	0.0022
10	217,666	1.5717	30	193	0.0014
11	162,878	1.1761	31	121	0.0009
12	121,345	0.8762	32	75	0.0005
13	89,988	0.6498	33	45	0.0003
14	66,418	0.4796	34	26	0.0002
15	48,771	0.3522	35	15	0.0001
16	35,620	0.2572	36	8	0.0001
17	25,873	0.1868	37	4	0.0000
18	18,678	0.1349	38	2	0.0000
19	13,398	0.0967	39	1	0.0000

Table 4. Multiplicity distribution, $dn/dN_{Z=3}$, of nuclear fragments with $Z = 3$ produced in $^{197}_{79}$Au fragmentation.

$N_{Z=3}$	$dn/dN_{Z=3}$	Fraction (%)	$N_{Z=3}$	$dn/dN_{Z=3}$	Fraction (%)
0	4,559,559	32.9242	14	9327	0.0673
1	3,103,402	22.4094	15	5468	0.0395
2	2,097,721	15.1475	16	3124	0.0226
3	1,408,279	10.1691	17	1760	0.0127
4	938,059	6.7736	18	956	0.0069
5	620,125	4.4779	19	512	0.0037
6	406,285	2.9338	20	259	0.0019
7	263,944	1.9059	21	130	0.0009
8	169,687	1.2253	22	59	0.0004
9	108,064	0.7803	23	27	0.0002
10	67,967	0.4908	24	10	0.0001
11	42,297	0.3054	25	4	0.0000
12	25,923	0.1872	26	1	0.0000
13	15,701	0.1134			

Table 5. Multiplicity distribution, $dn/dN_{Z=4}$, of nuclear fragments with $Z = 4$ produced in $^{197}_{79}$Au fragmentation.

$N_{Z=4}$	$dn/dN_{Z=4}$	Fraction (%)	$N_{Z=4}$	$dn/dN_{Z=4}$	Fraction (%)
0	5,730,386	41.3787	10	16,302	0.1177
1	3,421,059	24.7032	11	8041	0.0581
2	2,017,516	14.5683	12	3832	0.0277
3	1,174,190	8.4787	13	1755	0.0127
4	673,679	4.8646	14	765	0.0055
5	380,544	2.7479	15	314	0.0023
6	211,333	1.5260	16	120	0.0009
7	115,189	0.8318	17	41	0.0003
8	61,493	0.4440	18	12	0.0001
9	32,076	0.2316	19	3	0.0000

Table 6. Multiplicity distribution, $dn/dN_{Z=5}$, of nuclear fragments with $Z = 5$ produced in $^{197}_{79}$Au fragmentation.

$N_{Z=5}$	$dn/dN_{Z=5}$	Fraction (%)	$N_{Z=5}$	$dn/dN_{Z=5}$	Fraction (%)
0	6,759,150	48.8073	8	18,875	0.1363
1	3,535,155	25.5271	9	7745	0.0559
2	1,812,715	13.0895	10	2990	0.0216
3	909,810	6.5697	11	1085	0.0078
4	445,665	3.2181	12	355	0.0026
5	212,630	1.5354	13	105	0.0008
6	98,350	0.7102	14	25	0.0002
7	43,990	0.3176	15	5	0.0000

Table 7. Multiplicity distribution, $dn/dN_{Z=6}$, of nuclear fragments with $Z = 6$ produced in $^{197}_{79}$Au fragmentation.

$N_{Z=6}$	$dn/dN_{Z=6}$	Fraction (%)	$N_{Z=6}$	$dn/dN_{Z=6}$	Fraction (%)
0	7,662,961	55.3336	7	14,795	0.1068
1	3,506,000	25.3165	8	4884	0.0353
2	1,558,184	11.2515	9	1468	0.0106
3	670,229	4.8397	10	389	0.0028
4	277,751	2.0056	11	86	0.0006
5	110,264	0.7962	12	14	0.0001
6	41,624	0.3006	13	1	0.0000

Table 8. Multiplicity distribution, $dn/dN_{Z=7}$, of nuclear fragments with $Z = 7$ produced in $^{197}_{79}$Au fragmentation.

$N_{Z=7}$	$dn/dN_{Z=7}$	Fraction (%)	$N_{Z=7}$	$dn/dN_{Z=7}$	Fraction (%)
0	8,455,867	61.0591	6	16,033	0.1158
1	3,380,225	24.4083	7	4349	0.0314
2	1,297,338	9.3680	8	1024	0.0074
3	475,277	3.4319	9	201	0.0015
4	164,768	1.1898	10	28	0.0002
5	53,538	0.3866	11	2	0.0000

Table 9. Multiplicity distribution, $dn/dN_{Z=8}$, of nuclear fragments with $Z = 8$ produced in $^{197}_{79}$Au fragmentation.

$N_{Z=8}$	$dn/dN_{Z=8}$	Fraction (%)	$N_{Z=8}$	$dn/dN_{Z=8}$	Fraction (%)
0	9,151,445	66.0819	5	24,343	0.1758
1	3,191,706	23.0471	6	5587	0.0403
2	1,054,223	7.6125	7	1079	0.0078
3	326,522	2.3578	8	161	0.0012
4	93,569	0.6757	9	15	0.0001

Table 10. Multiplicity distribution, $dn/dN_{Z=9}$, of nuclear fragments with $Z = 9$ produced in $^{197}_{79}$Au fragmentation.

$N_{Z=9}$	$dn/dN_{Z=9}$	Fraction (%)	$N_{Z=9}$	$dn/dN_{Z=9}$	Fraction (%)
0	9,760,682	70.4811	5	10,352	0.0748
1	2,966,463	21.4206	6	1727	0.0125
2	839,916	6.0650	7	216	0.0016
3	218,328	1.5765	8	15	0.0001
4	50,951	0.3679			

Table 11. Multiplicity distribution, $\mathrm{d}n/\mathrm{d}N_{Z=10}$, of nuclear fragments with $Z = 10$ produced in $^{197}_{79}$Au fragmentation.

$N_{Z=10}$	$\mathrm{d}n/\mathrm{d}N_{Z=10}$	Fraction (%)	$N_{Z=10}$	$\mathrm{d}n/\mathrm{d}N_{Z=10}$	Fraction (%)
0	10,294,305	74.3344	4	26,620	0.1922
1	2,722,525	19.6591	5	4075	0.0294
2	658,295	4.7535	6	460	0.0033
3	142,340	1.0278	7	30	0.0002

Table 12. Multiplicity distribution, $\mathrm{d}n/\mathrm{d}N_{Z=11}$, of nuclear fragments with $Z = 11$ produced in $^{197}_{79}$Au fragmentation.

$N_{Z=11}$	$\mathrm{d}n/\mathrm{d}N_{Z=11}$	Fraction (%)	$N_{Z=11}$	$\mathrm{d}n/\mathrm{d}N_{Z=11}$	Fraction (%)
0	10,760,915	77.7037	4	13,308	0.0961
1	2,473,581	17.8615	5	1474	0.0106
2	508,596	3.6725	6	99	0.0007
3	90,675	0.6548	7	2	0.0000

Table 13. Multiplicity distribution, $\mathrm{d}n/\mathrm{d}N_{Z=12}$, of nuclear fragments with $Z = 12$ produced in $^{197}_{79}$Au fragmentation.

$N_{Z=12}$	$\mathrm{d}n/\mathrm{d}N_{Z=12}$	Fraction (%)	$N_{Z=12}$	$\mathrm{d}n/\mathrm{d}N_{Z=12}$	Fraction (%)
0	11,168,961	80.6502	4	6352	0.0459
1	2,228,413	16.0912	5	475	0.0034
2	388,015	2.8018	6	15	0.0001
3	56,419	0.4074			

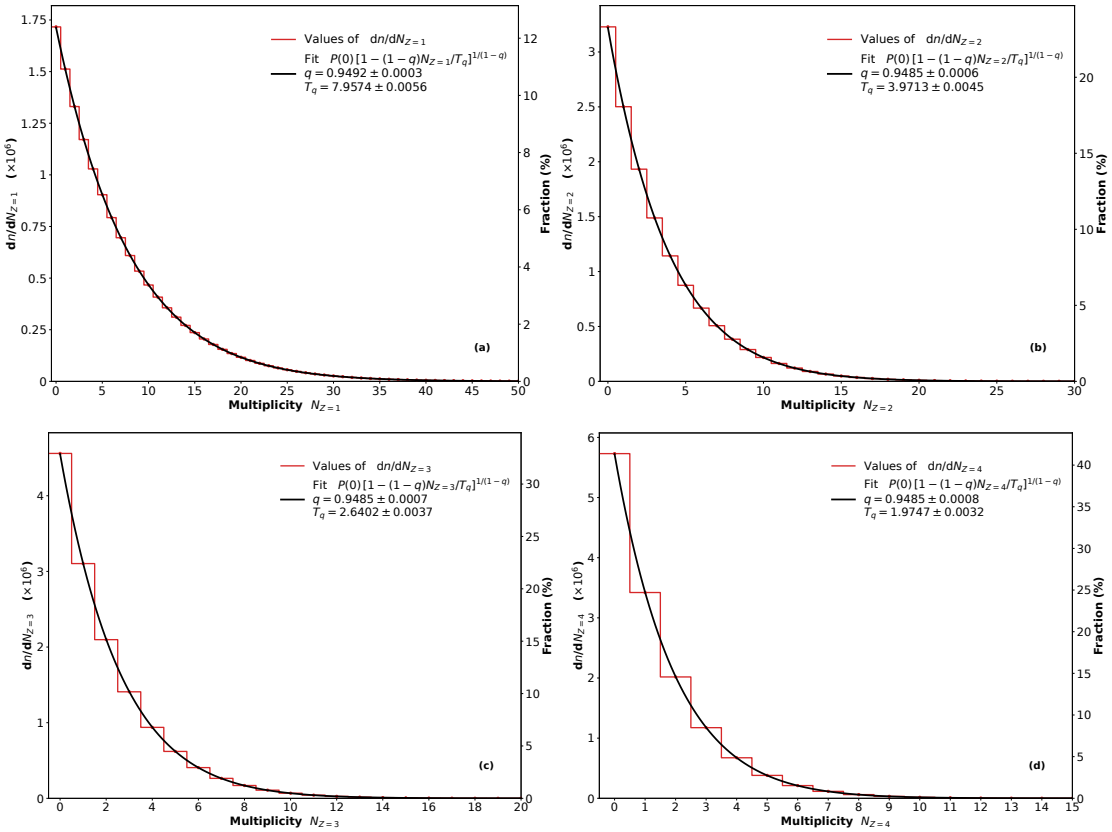


Figure 2. *Cont.*

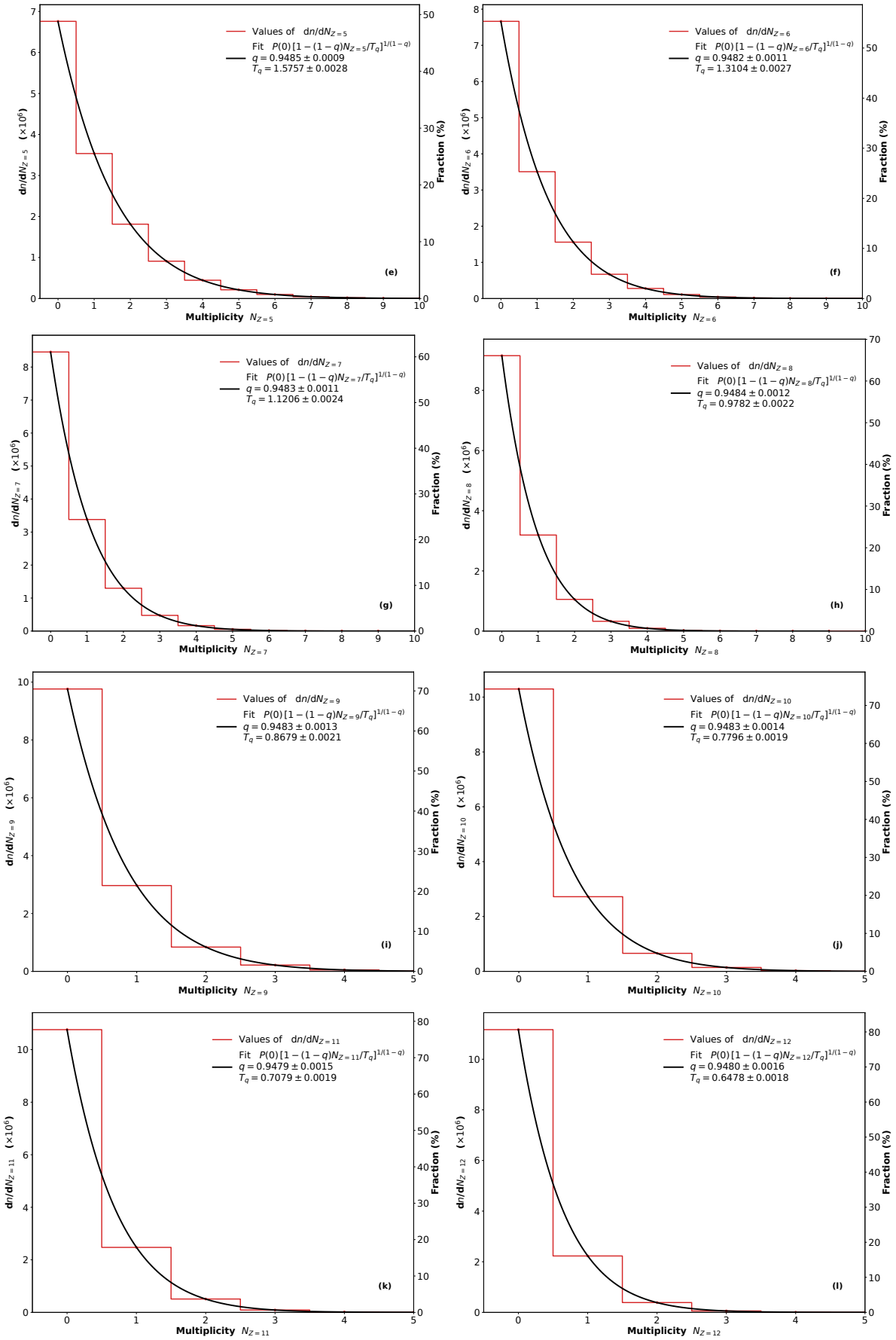


Figure 2. Multiplicity distributions, $\mathrm{d}n/\mathrm{d}N_Z$, of nuclear fragments with charge Z obtained from the combinatorial baseline for the fragmentation of $^{197}_{79}$Au. The histogram shows the ex-

act values of $\mathrm{d}n/\mathrm{d}N_Z$ obtained from the equiprobable charge-partition method. The right vertical axis gives the percentage fraction (%). The curves are fits using the Tsallis function $P(N_Z) = P(0)[1-(1-q)N_Z/T_q]^{1/(1-q)}$ over the available multiplicity ranges. Panels (**a**–**l**) correspond to $Z = 1$–12. The fitted parameters (q and T_q) are given in the legend of each panel, with $P(0) = \mathrm{d}n/\mathrm{d}N_Z|_{N_Z=0}$. Because the combinatorial baseline yields exact and error-free values for $\mathrm{d}n/\mathrm{d}N_Z$, standard statistical p-value tests cannot be used to assess the goodness of fit. However, to estimate the parameter uncertainties, we apply the χ^2 profile method by artificially assigning Poisson statistical uncertainties ($\sqrt{\mathrm{d}n/\mathrm{d}N_Z}$) to the exact baseline yields. The reported uncertainties assume a 1σ deviation corresponding to a 68.3% confidence level.

3. Dependence of Empirical Parameters on Beam Atomic Number

The preceding analysis of gold fragmentation serves as an illustrative mathematical example. In what follows, we apply the same partition method to study the multiplicity distributions of nuclear fragments with $Z = 1$ and 2 produced in the fragmentation of nuclei with $Z_{\mathrm{beam}} = 6$–100, in order to extract the values of the empirical fitting parameters q and T_q and investigate their dependence on Z_{beam}. It must be emphasized that q and T_q here are extracted from the idealized combinatorial baseline, not from real experimental data influenced by collective dynamics. We did not choose very light nuclei with $Z_{\mathrm{beam}} < 6$ because their low-multiplicity distributions are insufficient to support a sufficiently large number of degrees of freedom (ndf) when fitting with the Tsallis function, which contains multiple free parameters. Since the multiplicity distributions involve too many tables and figures, we do not include them in the paper; instead, we directly present the fitted q-Z_{beam} and T_q-Z_{beam} relations, shown in Figure 3a and Figure 3b, respectively. In these figures, circles represent the results for $Z = 1$, squares represent the results for $Z = 2$, and the dashed line in Figure 3a corresponds to $q = 1$. To better observe the trend, the results for $Z_{\mathrm{beam}} = 6$–50, indicated by the dotted rectangle in Figure 3a, are extracted and displayed enlarged in an inset in the upper right.

As Z_{beam} increases, the fitted q parameter first decreases rapidly from values greater than 1 to a minimum below 1, and then increases with increasing Z_{beam}, but never reaches 1. The results for $Z = 1$ and 2 show no obvious difference. Meanwhile, the fitted T_q parameter increases monotonically with Z_{beam}, and the value for $Z = 2$ is about twice that for $Z = 1$.

We note that the error bars of q and T_q extracted from light nuclei ($Z_{\mathrm{beam}} = 6$–20) are very large. This is because the limited multiplicity leads to a limited number of degrees of freedom compared with the number of parameters. In this small-system regime, a few fitted values of q exceed 1. This is a mathematical artifact of the fitting procedure applied to the combinatorial distributions with sparse multiplicity, rather than an indication of genuine nonextensive thermodynamic behavior or thermal excitation in physical fragmentation processes. Because our baseline model contains no dynamical or thermal mechanisms, one must avoid assigning direct physical interpretations (such as long-range correlations or collective flow) to these extreme cases where $q > 1$.

We now analyze the trends of the empirical fitting parameters (q and T_q). To investigate these trends for very heavy nuclei, we restrict our analysis to cases with $Z_{\mathrm{beam}} \geq 20$. In Figure 4a, the q-Z_{beam} relation is plotted with a narrow vertical range (0.86–1.02) and a wide horizontal range (0–300). Circles and squares denote the results for $Z = 1$ and 2, respectively. The function expressed as

$$q = 1 - aZ_{\mathrm{beam}}^{-b} \tag{7}$$

is used to fit the $Z = 1$ and $Z = 2$ results over $Z_{\mathrm{beam}} = 20$–100, yielding the solid and dashed curves, respectively. The fitted parameters a and b are shown in the panel together with χ^2/ndf, where ndf denotes the number of degrees of freedom. To better visualize the slope parameter (b), the relation between $\ln(1-q)$ and $\ln Z_{\mathrm{beam}}$ for $Z_{\mathrm{beam}} = 20$–100 is

presented in Figure 4b. The two sets of parameters are almost identical within the error ranges. When the fitted curve is extrapolated to $Z_{\mathrm{beam}} = 300$, q remains less than 1; this mathematical trend indicates that q will stay below 1 even for higher Z_{beam} values. This behavior is a direct mathematical consequence of the finite combinatorial space: as the system size increases, the distribution's support becomes larger, but the constraint of charge conservation inherently limits the multiplicity range, ensuring $q < 1$ for the compact-support Tsallis fit. A clear linear relation between $\ln(1-q)$ and $\ln Z_{\mathrm{beam}}$, i.e., a double-logarithmic relation between $1-q$ and Z_{beam}, is observed.

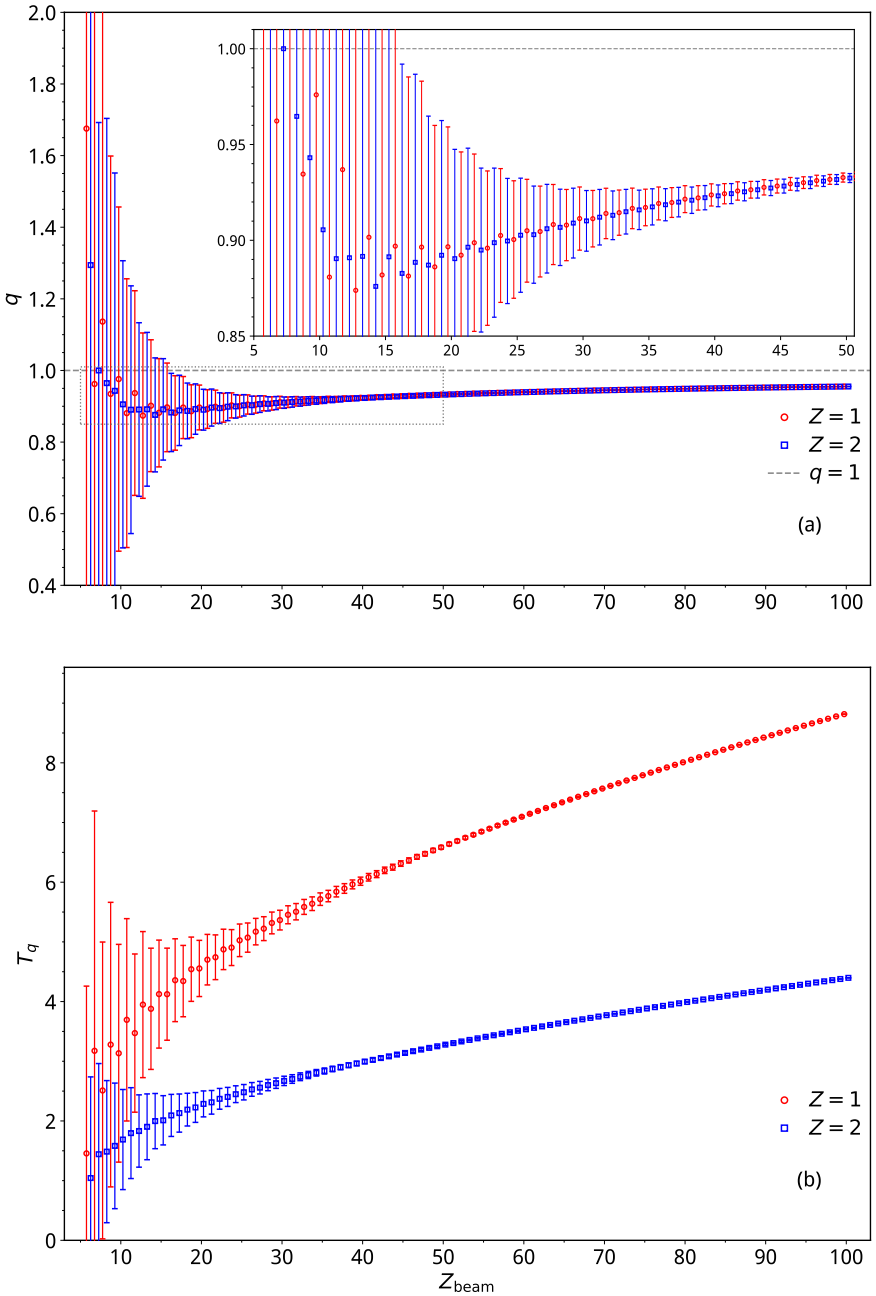


Figure 3. (**a**) The q-Z_{beam} relation and (**b**) the T_q-Z_{beam} relation. Circles and squares denote the results for $Z = 1$ and $Z = 2$, respectively. The dashed line in panel (**a**) corresponds to $q = 1$. The results for $Z_{\mathrm{beam}} = 6$–50, marked by the dotted rectangle in panel (**a**), are displayed enlarged in an inset in the upper part, slightly to the right. The vertical line segments represent the error bars described in the caption of Figure 2.

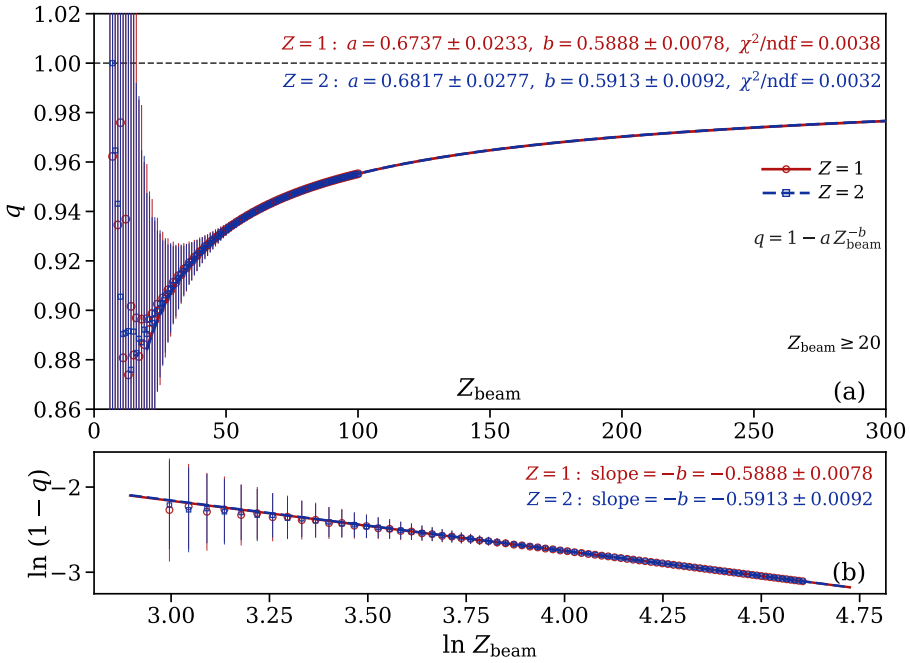


Figure 4. (**a**) The q-Z_{beam} relation, shown over a narrow vertical range (0.86–1.02) and a wide horizontal range (0–300). Circles and squares denote the $Z = 1$ and $Z = 2$ results, respectively. The solid and dashed curves are fits to the $Z = 1$ and $Z = 2$ results, respectively, using $q = 1 - aZ_{\mathrm{beam}}^{-b}$ for $Z_{\mathrm{beam}} = 20$–100. The horizontal dashed line represents $q = 1$ and the vertical line segments represent the error bars described in the caption of Figure 2. (**b**) The $\ln(1 - q)$–$\ln Z_{\mathrm{beam}}$ relation for $Z_{\mathrm{beam}} = 20$–100. The uncertainties of the parameters are obtained from the χ^2 profile method, assuming a 1σ deviation corresponding to a 68.3% confidence level.

Figure 5a shows the T_q-Z_{beam} relation over wide ranges on both axes. Circles and squares denote the results for $Z = 1$ and 2, respectively. The function expressed as

$$T_q = A\sqrt{Z_{\mathrm{beam}}} + B \tag{8}$$

is used to fit the $Z = 1$ and $Z = 2$ results over $Z_{\mathrm{beam}} = 20$–100, yielding the solid and dashed curves, respectively. The fitted values of A and B are shown in the panel together with χ^2/ndf. To better visualize the dependence, the T_q versus $\sqrt{Z_{\mathrm{beam}}}$ relation for $Z_{\mathrm{beam}} = 20$–100 is presented in Figure 5b. The two sets of parameters are clearly different. When the fitted curve is extrapolated to $Z_{\mathrm{beam}} = 300$, T_q continues to increase, and this trend is expected to persist mathematically at higher Z_{beam}. A clear linear relation between T_q and $\sqrt{Z_{\mathrm{beam}}}$ is observed. This scaling relation characterizes the geometric growth of the combinatorial phase space rather than a physical temperature. However, this baseline scaling provides a valuable zero-order reference: future experimental measurements, which will be strongly modified by radial collective expansion and reaction dynamics, can be compared against this pure combinatorial limit to isolate and quantify the magnitude of collective effects in the fragmentation process.

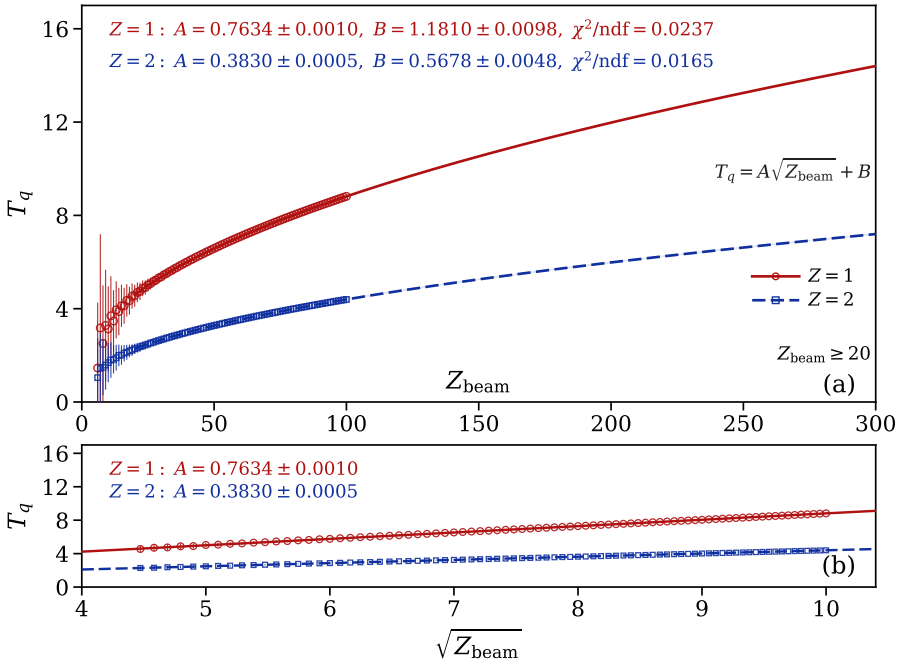


Figure 5. (**a**) The T_q-Z_{beam} relation, plotted over wide ranges on both axes. Circles and squares denote the $Z = 1$ and $Z = 2$ results, respectively. The solid and dashed curves are fits to the $Z = 1$ and $Z = 2$ results, respectively, using $T_q = A\sqrt{Z_{\mathrm{beam}}} + B$ for $Z_{\mathrm{beam}} = 20$–100. The vertical line segments represent the error bars described in the caption of Figure 2. (**b**) The T_q versus $\sqrt{Z_{\mathrm{beam}}}$ relation for $Z_{\mathrm{beam}} = 20$–100. The uncertainties of the parameters are obtained from the χ^2 profile method, assuming a 1σ deviation corresponding to a 68.3% confidence level.

4. Discussion

The present results show that the multiplicity distributions of nuclear fragments in the combinatorial fragmentation baseline are well described by a q-exponential with $q \approx 0.948 < 1$. It is crucial to emphasize that this mathematical property arises purely from the combinatorial constraint of a finite charge space. Although the distributions are well reproduced by the Tsallis form, this does not establish that the physical system itself obeys nonextensive statistics. The $q < 1$ parameter mathematically indicates a compact-support distribution intrinsic to the finite phase space of integer partitions. It reflects a truncation effect originating from the finite combination of charge numbers, rather than a genuine new nonextensive thermodynamic mechanism.

The significance of this study lies mainly in its provision of an idealized reference point, rather than a complete physical description. (i) We map the well-developed integer partition theory to the charge fragmentation of high-energy nuclei under the strict assumption of equiprobable channels. This establishes a purely combinatorial, zero-free-parameter baseline that isolates global charge conservation from complex dynamics. (ii) The compact-support shape ($q < 1$) of the resulting multiplicity distribution is naturally obtained at the geometric–statistical level without introducing dynamical correlations. This provides a mathematical correspondence that can serve as a baseline for understanding the Tsallis-like fits often applied to real data. (iii) This baseline provides an unbiased theoretical reference for future nuclear fragmentation experiments at the EIC. The deviation of experimentally measured yields from this equiprobable partition baseline indicates the presence of non-combinatorial physical effects, offering a comparative tool for investigating underlying dynamics.

The central advantage of the equivalence proposed here is that it establishes a parameter-free benchmark. Traditional statistical fragmentation models require at least

five free parameters, such as temperature, fragmentation excitation energy, fragment formation energy, etc., to fit experimental data. Parameter values reported by different research groups vary widely, severely limiting the predictive power of these models [11–14]. While our model does not replace these dynamical descriptions, it provides an idealized limit. Any deviation of real fragmentation data from this baseline can be attributed to non-combinatorial effects (such as reaction dynamics, phase-space weights, and collective expansion). This helps to constrain and benchmark the physical interpretations of parameters in traditional models.

Concerning the mathematical properties of the partition ensemble, the statistical ensemble formed by all equiprobable partitions exhibits a highly non-linear, explosive growth in the total number of states. For a given integer, splitting it into two parts does not simply add their respective partition numbers. In fact, if one defines the combinatorial entropy as the logarithm of the number of states, this entropy strictly exhibits subadditivity. We stress that this is purely a property of the mathematical state space, not a proof of the physical entropy evolution of the nuclear system. The compact-support distribution corresponding directly to $q < 1$ does not invoke additional dynamical correlation assumptions. It predicts that the baseline multiplicity distribution is a finite-size compact-support process originating from the geometric–statistical properties of the fragmentation-channel space, providing an analytically solvable example for combinatorial finite systems.

In addition, this equivalence framework provides a rigorous mathematical lower bound for the statistical description of nuclear fragmentation: for any physical fragmentation model satisfying charge conservation, the distribution of fragmentation channels is defined over this combinatorial space; dynamical effects can only reweight the channel probabilities relative to the uniform distribution. This provides a practical theoretical reference for the fragmentation-channel yield data in EIC experiments. Any experimental data that deviate significantly from this reference indicate the presence of dynamical mechanisms; for example, a liquid–gas phase transition or α-particle clustering would introduce specific deviations from the baseline predictions. The former implies a substantial number of light fragments ($Z = 1$ and $Z = 2$), whereas the latter indicates a high yield of $Z = 2$ fragments.

Regarding future applications, the method discussed in this paper has broad prospects for data analysis of future nuclear fragmentation experiments at the EIC [1–6]. By comparing the experimentally measured fragmentation yields with this baseline, one can isolate deviations that reflect the dynamical preference of different channels. While these deviations are linked to preformation probabilities and cluster structures, quantitative extraction of such physical quantities requires the incorporation of advanced dynamical models alongside this baseline. Extending the partition theory from one-dimensional charge-number partitions to two-dimensional joint charge-number–mass-number partitions would further provide baseline predictions for isotope yield distributions, giving a theoretical reference for exotic-nucleus production experiments at the EIC.

Furthermore, a profound dynamical connection exists between the nuclear fragmentation baseline and collectivity. Collectivity, especially radial collective expansion, acts as a key driving force for real nuclear fragmentation. In actual collisions, the hot and dense nuclear matter formed at the initial stage converts thermal energy into ordered radial kinetic energy during the expansion phase. When this collective expansion is sufficiently violent, the system density drops rapidly and enters a mechanically unstable (spinodal) region, subsequently disintegrating into multiple intermediate-mass fragments. Experimentally, the radial collective energy extracted from fragment energy spectra shows a positive correlation with fragment multiplicity. In high-energy collisions, while the participant region is dominated by strong collective flow, the fragmentation of the spectator region is also heavily influenced by collective expansion. Therefore, comparing real experimental data with our

idealized combinatorial baseline allows us to isolate these collective and dynamical effects. The deviation from the equiprobable partition baseline provides a quantitative reference for extracting parameters of radial collective flow and understanding the complete evolutionary picture of nuclear matter from a continuous medium to discrete fragments.

It should be noted that the framework proposed in this work is a pure, idealized combinatorial baseline that strictly isolates global charge conservation, and does not include nuclear interactions, collective expansion, or reaction dynamics. A direct comparison with low-energy experimental data would inevitably result in profound discrepancies, as the underlying physics involves complex dynamical evolutions absent in our baseline. In addition, at low energies, the nucleus is typically only partially excited rather than completely fragmented. The reason we emphasize future EIC experiments is that EIC provides a unique environment of high-energy deep inelastic scattering, where the fragmentation of the spectator region is driven by completely different kinematic conditions. Therefore, we agree that a future step should involve applying our baseline to future high-energy datasets by integrating it with dynamical models to quantify these discrepancies.

Regardless of how high the excitation energy is, our model inherently does not depend on the excitation energy of the nucleus. This is indeed a severe limitation when describing real experimental fragmentation. We want to clarify that this insensitivity to excitation energy is an intrinsic feature of the pure combinatorial baseline, not a physical claim. In reality, the excitation energy dictates the available phase space, thermal expansion, and the subsequent disassembly of the nucleus. When the excitation energy is relatively low, the nucleus is only partially fragmented, and the combinatorial model applies solely to the fragmented part. When the excitation energy is high enough to completely fragment the nucleus, the model applies to the whole nucleus, and at this point, further increasing the excitation energy will not affect the model's results. Because our model only counts the discrete charge partitions without any thermodynamic weighting (such as Boltzmann factors or phase-space integrals), it cannot naturally reproduce the excitation-energy dependence. Instead, the deviation of experimental data (at various excitation energies) from our baseline can exactly capture the dynamical and thermal effects induced by excitation energy. Therefore, our parameter-free baseline serves as a zero-excitation reference, allowing future studies to isolate the true thermodynamic impact of excitation energy on the fragmentation process.

Although models such as the Statistical Multifragmentation Model (SMM) are highly valuable because they incorporate physical parameters (e.g., temperature, freeze-out volume, and excitation energy) [29,30] to reveal detailed physical processes within the excited nuclear matter, the strength of SMM and similar models is also their weakness. For example, the extracted physical conclusions are highly sensitive to the chosen phenomenological parameters. The advantage of our parameter-free model is that it provides a rigorous, unbiased mathematical benchmark. It isolates the pure combinatorial geometry of charge conservation. From this baseline, one can extract the "dynamical deviation factor" for any specific fragmentation channel by comparing it with experimental data. This deviation factor quantifies how much the real physical system deviates from the pure uniform probability limit due to nuclear interactions and dynamics. It can serve as a clean, unbiased constraint to calibrate and benchmark the parameters used in SMM-like models, rather than replacing them.

As we know, physical Tsallis statistics typically imply long-range correlations, memory effects, or non-trivial phase-space configurations. However, our proposed model inherently contains none of these physical correlations. Our position is that the Tsallis-like parameter ($q < 1$) obtained in this work is strictly an empirical mathematical fitting parameter, not a physical manifestation of genuine non-extensivity. The mathematical reason for the emer-

gence of $q < 1$ is the compact support of the discrete integer partition space: the distribution has a hard cutoff at high multiplicity due to charge conservation. This hard geometric truncation mimics the mathematical form of a $q < 1$ Tsallis distribution. We emphasize that this is a finite-size combinatorial artifact. The physical origins of Tsallis statistics in real heavy-ion collisions (long-range correlations) are completely distinct from the pure combinatorial boundaries we have calculated. Our baseline simply demonstrates that finite combinatorial spaces can mathematically masquerade as non-extensive statistical systems.

Before the Summary and Conclusions, we would like to emphasize that the present framework is a purely statistical and combinatorial exercise, which does not introduce nuclear interactions or quantum many-body theories. This does not mean, however, that it is free of physical constraints: we have taken into account the conservation of the fragment charge number, so that the fragment charges in every admissible partition sum to Z_{beam}, and this constraint is imposed on the construction rather than fitted to data. In this study, our goal is not to provide a complete dynamical explanation of experimental fragmentation yields, but rather to establish a rigorous, parameter-free zero-order baseline. Real fragmentation processes are governed by complex quantum many-body dynamics, nuclear forces, and collective expansion. By providing a pure combinatorial baseline where all charge partitions are strictly equiprobable, we impose the sole physical constraint of fragment charge-number (Z_i) conservation, $\sum_i Z_i = Z_{\mathrm{beam}}$, and thereby isolate its effect from that of all other ingredients. The deviations between actual experimental data and this idealized baseline precisely encapsulate the missing physics, including nuclear interactions, dynamical fluctuations, and collective effects. Therefore, we do not claim that this combinatorial model can directly explain experimental data; rather, the present work provides a benchmark to which readers may refer when considering the physical problem with a fuller set of ingredients so that dynamical models and experimental yields can be quantitatively compared against it to extract non-combinatorial physical information.

In addition, it is crucial to emphasize that the T_q parameter extracted in our work is not a thermodynamic temperature in the physical sense but an empirical parameter characterizing the mathematical shape of the combinatorial partition distribution. In a purely combinatorial charge partition space, as the beam charge number (Z_{beam}) increases, the phase space of available states undergoes a geometric expansion, causing a systematic change in the shape of the multiplicity distribution. This directly leads to the scaling behavior of $T_q \propto \sqrt{Z_{\mathrm{beam}}}$. The sensitivity of T_q to Z_{beam} is therefore a mathematical reflection of the growing combinatorial state space, not a physical temperature variation. Moreover, thermal and chemical equilibrium is a standard assumption for the freeze-out stage of heavy-ion collisions. The discrepancy between the purely geometric T_q scaling obtained here and the physical freeze-out temperature extracted from experiments further highlights the presence of complex physical dynamics (such as collective expansion), which are not captured by our idealized combinatorial baseline. It is precisely in this discrepancy, obtained while fragment charge-number conservation remains exactly satisfied, that the idealized construction becomes useful as a benchmark for physical considerations rather than as a description of the freeze-out stage itself.

The sense in which this zero-order construction serves as a benchmark is worth stating precisely. Subject to $\sum_i Z_i = Z_{\mathrm{beam}}$ and to the strict equiprobability of admissible charge partitions, the baseline attributes any structure in the multiplicity distribution to combinatorics alone. It is therefore a null reference rather than a competing description of a particular fragmentation process. For readers who approach the physical problem with nuclear interactions, dynamical fluctuations or collective expansion included, this reference remains of practical use: an added ingredient is informative to the extent that it moves the predicted yields away from the baseline, and the magnitude and location of that departure

indicate where a physical explanation is actually required. The value of the simplification lies here, in being simple enough to be used as a controlled reference while still respecting a constraint that any more detailed description must equally obey.

Several questions are left open, and the present formulation makes them well-posed. The first concerns how the charge-conserving combinatorial baseline is to be linked to concrete physical problems, in particular to specified fragment-charge observables and to the conditions under which the zero-order description may be expected to apply. The second concerns how it may offer a directional reference for future studies: once the baseline is fixed, the deviations identified above indicate the regimes in which nuclear interactions or collective dynamics are called for, and those in which further elaboration would merely reproduce what the combinatorial construction already yields, so that the geometric $T_q \propto \sqrt{Z_{\mathrm{beam}}}$ scaling can be read as a direction indicator rather than as a physical temperature. The third concerns the discussion itself, namely what level of physical detail a statistical baseline of this kind should carry, and whether a carefully delimited zero-order reference is a result in its own right or only a starting point. We do not attempt to settle these questions here. By stating them alongside a reproducible, charge-conserving reference case, we hope the present work invites others working on fragmentation to take a position and thereby helps to open the question to broader discussion.

5. Summary and Conclusions

This paper establishes a mathematical mapping between integer partitions and nuclear fragmentation channels when only charge-number conservation is considered. Each partition of the charge number is shown to correspond to an independent fragmentation channel, and under the idealized prior assumption of no dynamical preference, all channels are set to be equiprobable. On this basis, we calculate exactly the full partition-number distribution for the gold nucleus with $Z_{\mathrm{beam}} = 79$ at the EIC, obtain the baseline multiplicity distribution, and enumerate all fragmentation channels. The multiplicity distributions of fragments with $Z = 1$ to $Z = 12$ are completely counted, yielding exact combinatorial results.

Using the same method, we applied this combinatorial framework to nuclei with charge numbers of $Z_{\mathrm{beam}} = 6$–100. From the multiplicity distributions of light fragments, we obtained the dependence of the empirical Tsallis fitting parameters (q and T_q) on Z_{beam}. In the range of $Z_{\mathrm{beam}} = 20$–100, the results are well described by

$$q = 1 - aZ_{\mathrm{beam}}^{-b}, \qquad T_q = A\sqrt{Z_{\mathrm{beam}}} + B.$$

For fragments with $Z = 1$ and $Z = 2$, the obtained q values are consistent and both less than 1, whereas the T_q value for $Z = 1$ is about twice that for $Z = 2$. When extrapolated to $Z_{\mathrm{beam}} = 300$, q approaches 1 more closely but remains less than 1, while T_q continues to increase. These trends characterize the geometric expansion of the combinatorial state space.

The results of this paper show that the multiplicity distribution based on equiprobable partitions mathematically exhibits compact-support characteristics and deviates from standard extensive Boltzmann statistics. The empirical Tsallis fit yields q significantly less than 1, which reflects the finite combinatorial nature of the charge partition space. This work relies on no phenomenological free parameters and provides a new baseline theoretical framework for analyzing nuclear fragmentation data. In the future, it can be used to isolate genuine dynamical and collective effects in fragmentation data from the EIC and other nuclear physics facilities, offering new research perspectives for exploring the internal structure of nuclei and the interplay between combinatorial constraints and strong interaction dynamics.

https://doi.org/10.3390/universe12110355

Author Contributions: Conceptualization, J.-Y.C. and C.-H.S.; methodology, J.-Y.C. and C.-H.S.; software, J.-Y.C.; validation, J.-Y.C. and C.-H.S.; formal analysis, J.-Y.C. and C.-H.S.; investigation, J.-Y.C. and C.-H.S.; resources, J.-Y.C. and C.-H.S.; data curation, J.-Y.C.; writing—original draft preparation, J.-Y.C.; writing—review and editing, J.-Y.C. and C.-H.S.; visualization, J.-Y.C. and C.-H.S.; supervision, C.-H.S.; project administration, J.-Y.C. and C.-H.S.; funding acquisition, J.-Y.C. and C.-H.S. All authors have read and agreed to the published version of the manuscript.

Funding: This research was funded by the Doctoral Research Startup Fund of Changzhi Medical College under Grant No. 2025BS45 and the Key Laboratory of Medical Electronics and Rehabilitation Device Engineering of Changzhi City under Grant No. 2023sy004.

Data Availability Statement: The data used to support the findings of this study are included within the article and are cited at relevant places within the text as references.

Acknowledgments: During the preparation of this manuscript, the authors used the DeepSeek-V4-Pro (official version 0813) only for the purposes of grammar/spelling correction and preliminary literature searches. Figures were generated in Python 3.15 (Matplotlib 3.10); plotting/analysis code was developed with assistance from Tencent's Yuanbao 2.62.0.632. All numerical values are exact. The authors have reviewed and edited the output and take full responsibility for the content of this publication.

Conflicts of Interest: The authors declare no conflicts of interest. The funder had no role in the design of the study; in the collection, analysis, or interpretation of the data; in the writing of the manuscript; or in the decision to publish the results.

References

1. Litvinenko, V.N.; Beebe-Wang, J.; Belomestnykh, S.; Ben-Zvi, I.; Blaskiewicz, M.M.; Calaga, R.; Chang X.Y.; Fedotov, A.; Gassner, D.; Hammons, L.; et al. High-energy high-luminosity Electron-Ion Collider eRHIC. *arXiv* **2011**, arXiv:1109.2819.
2. Abeyratne, S.; Accardi, A.; Ahmed, S.; Barber, D.; Bisognano, J.; Bogacz, A.; Castilla, A.; Chevtsov, P.; Corneliussen, S.; Deconinck, W.; et al. Science requirements and conceptual design for a polarized medium energy Electron-Ion Collider at Jefferson Lab. *arXiv* **2011**, arXiv:1209.0757.
3. Accardi, A.; Albacete, J.L.; Anselmino, M.; Armesto, N.; Aschenauer, E.C.; Bacchetta, A.; Boer, D.; Brooks, W.K.; Burton, T.; Chang, N.B.; et al. Electron Ion Collider: The next QCD frontier—Understanding the glue that binds us all. *arXiv* **2012**, arXiv:1212.1701.
4. Anderle, D.P.; Bertone, V.; Cao, X.; Chang, L.; Chang, N.B.; Chen, G.; Chen, X.R.; Chen, Z.J.; Cui, Z.F.; Dai, L.Y. et al. Electron-Ion Collider in China. *Front. Phys.* **2021**, *16*, 64701. [CrossRef]
5. Chen, X.R. A plan for Electron Ion Collider in China. *arXiv* **2018**, arXiv:1809.00448.
6. Xiao, B.W.; Zhao, Y.X.; Zhou, J. Physics of the Electron–Ion Collider in China. *Prog. Part. Nucl. Phys.* **2026**, *151*, 104264. [CrossRef]
7. Aschenauer, E.C.; Borsa, I.; Sassot, R.; Van Hulse, C. Semi-inclusive deep-inelastic scattering, parton distributions and fragmentation functions at a future Electron-Ion Collider. *Phys. Rev. D* **2019**, *99*, 094004 [CrossRef]
8. Hekhorn, F.; Magni, G.; Nocera, E.R.; Rabemananjara, T.R.; Rojo, J.; Schaus, A.; Stegeman, R. Heavy quarks in polarised deep-inelastic scattering at the Electron-Ion Collider. *Eur. Phys. J. C* **2024**, *84*, 189. [CrossRef]
9. Jentsch, A.; Tu, Z.D.M.; Weiss, C. Deep-inelastic electron-deuteron scattering with spectator nucleon tagging at the Electron-Ion Collider. Extracting free nucleon structure. *Phys. Rev. C* **2021**, *104*, 065205. [CrossRef]
10. Jain, S.; Aggarwal, R.; Kaur, M. Jet substructure in neutral current deep inelastic e+p scattering at upcoming Electron-Ion Collider. *Phys. Rev. D* **2023**, *107*, 116002. [CrossRef]
11. Souza, S.R.; Donangelo, R. Size properties of the largest fragments produced in the framework of the statistical multifragmentation model. *arXiv* **2020**, arXiv:2004.12860.
12. Mallik, S.; Chaudhuri, G.; Gulminelli, F. Dynamical and statistical bimodality in nuclear fragmentation. *Phys. Rev. C* **2018**, *97*, 024606. [CrossRef]
13. Souza, S.R.; Carlson, B.V.; Donangelo, R.; Lynch, W.G.; Tsang, M.B. Internal and kinetic temperatures of fragments in the framework of a nuclear statistical multifragmentation model. *Phys. Rev. C* **2015**, *92*, 024612. [CrossRef]
14. Urmossy, K. Jet mass dependence of fragmentation in positron-proton collisions. *Eur. Phys. J. A* **2017**, *53*, 36. [CrossRef]
15. Tsallis, C. Possible generalization of Boltzmann–Gibbs statistics. *J. Stat. Phys.* **1988**, *52*, 479–487. [CrossRef]
16. Tsallis C. Nonadditive entropy and nonextensive statistical mechanics—An overview after 20 years. *Braz. J. Phys.* **2009**, *39*, 337–356. [CrossRef]
17. Biró, T.S.; Purcsel G.; Urmössy, K. Non-extensive approach to quark matter. *Eur. Phys. J. A* **2009**, *40*, 325. [CrossRef]

18. Cleymans, J.; Paradza, M.W. Tsallis statistics in high energy physics: Chemical and thermal freeze-outs. *Physics* **2020**, *2*, 654–664. [CrossRef]
19. Parvan, A.S. Equivalence of the phenomenological Tsallis distribution to the transverse momentum distribution of q-dual statistics. *Eur. Phys. J. A* **2020**, *56*, 106. [CrossRef]
20. Tsang, C.Y.; Xu, Z. Mass-dependent non-extensivity in Tsallis blast-wave fits to identified hadron p_T spectra at RHIC and LHC. *arXiv* **2026**, arXiv:2606.24777.
21. Andrews, G.E. *The Theory of Partitions*; Encyclopedia of Mathematics and Its Applications, Volume 2; Addison-Wesley Publishing Company: Reading, MA, USA, 1976.
22. Chen, Y.H.; He, T.Y.; Tang, F.; Wei, J.J. Some separable integer partition classes. *Int. J. Number Theory* **2024**, *20*, 1353–1371. [CrossRef]
23. He, T.Y.; Huang, C.S.; Li, H.X.; Zhang, X. Separable integer partition classes and partitions with congruence conditions. *Ramanujan J.* **2025**, *67*, 36. [CrossRef]
24. Sloane, N.J.A. The On-Line Encyclopedia of Integer Sequences. Available online: https://oeis.org/A008284/b008284.txt (accessed on 10 September 2026).
25. Bonamente, M. Three Fundamental Distributions: Binomial, Gaussian, and Poisson. In *Statistics and Analysis of Scientific Data*, 2nd ed.; Bonamente, M., Ed.; Graduate Texts in Physics; Springer: New York, NY, USA, 2016. [CrossRef]
26. Gumbel, E.J. *Statistics of Extremes*; Columbia University Press: New York, NY, USA, 1958. [CrossRef]
27. Botet, R.; Płoszajczak, M. Fragmentation-inactivation binary model. *Phys. Rev. Lett.* **1992**, *69*, 3696–3699. [CrossRef]
28. Gruyer, D.; Frankland1, J.D.; Botet, R.; Płoszajczak, M.; Bonnet, E.; Chbihi, A.; Ademard, G.; Boisjoli, M.; Borderie, B.; Bougault, R.; et al. Nuclear multifragmentation time scale and fluctuations of the largest fragment size. *Phys. Rev. Lett.* **2013**, *110*, 172701. [CrossRef]
29. Lin, W.; Ren, P.; Zheng, H.; Liu, X.; Huang, M.; Wada, R.; Qu, G. Sensitivity study of experimental measures for the nuclear liquid-gas phase transition in the statistical multifragmentation model. *Phys. Rev. C* **2018**, *97*, 054615. [CrossRef]
30. Sagun, V.V.; Ivanytskyi, A.I.; Bugaev, K.A.; Mishustin, I.N. The statistical multifragmentation model for liquid-gas phase transition with a compressible nuclear liquid. *Nucl. Phys. A* **2014**, *924*, 24–46. [CrossRef]

Disclaimer/Publisher's Note: The statements, opinions and data contained in all publications are solely those of the individual author(s) and contributor(s) and not of MDPI and/or the editor(s). MDPI and/or the editor(s) disclaim responsibility for any injury to people or property resulting from any ideas, methods, instructions or products referred to in the content.